

Novel Coupled Electric Field Method for Defect Characterization in Eddy Current Non-destructive Testing Systems

T. Bouchala · B. Abdelhadi · A. Benoudjit

Received: 12 March 2013 / Accepted: 17 August 2013 / Published online: 11 September 2013
© Springer Science+Business Media New York 2013

Abstract This article presents a defect modeling in eddy current non-destructive testing systems by using a new developed method called coupled electric field. It permits to improve qualitatively several models developed so far by many authors using coupled circuit methods that consider the defect only as loss of material. However, a defect can occur with a finite conductivity such as impurity, small burns and micro-solder. For this reason, this investigation consists of extending the coupled circuit method to the modeling of this kind of defects. The proposed approach consists of firstly considering the defect as an electric conductive volume and secondly changing the state variable presenting the electric current by the electric field one. This procedure permits expressing explicitly the impedance variation caused by the presence of an axi-symmetrical defect according to its characteristics. The comparison between the impedance variations calculated using finite elements method and the proposed one demonstrates a very good concordance. After this validation, the study covers also the influence of the de-

fect shape and position on encircling probe impedance. This method is interesting since it permits a fully characterization of this kind of defects and facilitates the inversion process. Moreover, using a 3D finite element observation, this fast tool of simulation can be adapted for a fast phenomenological modeling of asymmetrical configurations.

Keywords Coupled electric field · Finite conductivity · Defect characterization · Eddy current · Non destructive testing · Inverse problem

1 Introduction

Eddy current non-destructive testing (EC-NDT) methods are used widely in aerospace, power and transportation industries where the cost of critical component failure can be high. This technique is one of the most extensively used for inspecting electric conductive materials at very high speeds because it does not require any contact between the test piece and the sensor [1]. The presence of the defect modifies the distribution of eddy current which causes alteration in the magnetic flux depending on the position and shape of the defects. Quantitative EC-NDE technique is needed for evaluating sizes, shapes, and locations of defects and cracks. A major aspect of current research is the inverse or defect characterization problems whose solution will allow the implementation of high speed automated testing equipment. The underlying assumptions in existing analytical models tend to invalidate any realistic application of the results to the problem of defect characterization in materials with complex defect boundaries or nonlinear physical characteristics. Besides, numerical methods are found to be accurate and applicable to any configurations (2D and 3D), but they are heavy and inadequate for a quick resolution of

T. Bouchala (✉) · B. Abdelhadi · A. Benoudjit
Electrical Engineering Department, El-Hadj Lakhdar University,
Batna, Algeria
e-mail: bouizra@yahoo.fr

B. Abdelhadi
e-mail: abdelhadi3b@yahoo.com

A. Benoudjit
e-mail: benoudjit@yahoo.fr

T. Bouchala · B. Abdelhadi · A. Benoudjit
Laboratory of Electric Traction Systems—Batna (LSTE—Batna),
Batna, Algeria

T. Bouchala
Electrical Engineering Department, Kasdi Merbah University,
Ouargla, Algeria

the inverse problems [2]. In this paper we propose a semi analytic method that we call coupled electric field method (CEFM) permitting to overcome these inconveniences. Several authors have applied the semi analytical methods for the modelling of axi-symmetrical configurations in which the defect is considered only as loss of material [3–11]. However, introducing the defect like an electric conductive volume has an immense utility, because it allows extending the coupled circuit method for other applications such as the detection of impurity, small burns and micro-solder [12, 13]. So, the main objective of this investigation is to manage to express the impedance variation according to defect geometrical (shape and size) and physical parameters, because during the manufacturing process and functioning operation of the conductive materials we need to detect and quantify several shapes of flaw. In fact, obtaining an explicit relation between the variation of impedance and parameters describing the defect shape remains a primordial objective [14, 15]. In order to establish this relation, the suggested approach consists of both formulating the coupled circuits equation expressing the defect as an electrically conductive volume and changing of the state variable presenting the electric current by the electric field one. In fact, the developed model is very important since it permits to solve quickly the inverse problem and allows a full characterization of the defect when the measured quantities are known [2].

2 Coupled Circuits Formulation

By using the coupled circuit notion, the electromagnetic phenomenon is described by generalized punctual equation (1) [3, 16].

$$\frac{2\pi r_p}{\sigma_p} J_p + \mu_o r_p G_{pq} \frac{dI_q(t)}{dt} = u_p \quad (1)$$

$$G_{pq} = \sqrt{\frac{r_p}{r_q}} E(k) \quad (2)$$

$$E(k) = \frac{(2 - k^2)E_1(k) - 2E_2(k)}{k} \quad (3)$$

$$k = \sqrt{\frac{4r_p r_q}{(r_p + r_q)^2 + (z_p - z_q)^2}} \quad (4)$$

where G_{pq} is called Green's function and represents the response of the system at a point $p(r_p, z_p)$ to Dirac's distribution located at a point $q(r_q, z_q)$. $E_1(k)$ and $E_2(k)$ are respectively the first and the second species of the Legendre elliptic function [3–6].

Equation (1) expresses the creation of the current density J_p at a point p of electric conductivity σ_p under the influence of the voltage u_p applied at this point, and the current intensity J_q situated at the point q .

The previous equation describes only the electromagnetic effect of one point upon another. To realize the electromagnetic contribution of the complete domain Ω upon point p , Eq. (1) is rewritten in the following form:

$$\frac{2\pi r_p}{\sigma_p} J_p + j\omega\mu_o r_p \iint_{\Omega} G_{pq} J_q d\Omega = u_p \quad (5)$$

3 Coupled Electric Field Formulation

The problem consists in expressing the inductive phenomenon according to the electric field. The utility of the state variable transformation resides in the electromagnetic problem type to be treated. In our case, this transformation allows expressing the eddy current probe impedance variation, caused by the presence of a defect, according to its physical and dimensional characteristics.

The current density J_p can be expressed according to the electric field E_p as follows:

$$\begin{cases} J_p = \sigma_p E_p \\ I_p = s_p \sigma_p E_p \end{cases} \quad (6)$$

s_p is the cross section of the turn p .

By introducing the transformation of equation group (6), Eq. (5) leads to Eq. (7). We have named this latter the generalized coupled electric field equation:

$$2\pi r_p E_p + j\omega\mu_o r_p \iint_{\Omega} G_{pq} \sigma_p E_p d\Omega = u_p \quad (7)$$

3.1 Geometrical Model and Description

Different coil probe structures are available to detect a large variety of cracks. In general, coil probes provide high crack sensitivity when eddy current flow is strongly altered by discontinuities. Pancake-type probes are formed of coils whose axis is perpendicular to the surface of the tested piece. When a penetrating crack occurs on the surface, current flow is strongly altered and the crack can be detected. Another probe type is the encircling-coil. This latter is sensitive to parallel discontinuities to the axis of the tube or rods as eddy currents follow around the radial circumferences in an opposing direction of coil currents around the energized coil current. Figure 1 presents a geometric configuration of an axially symmetric electromagnetic system. This latter includes a source of domain Ω_o which delivers a sinusoidal voltage, and a massive piece of domain Ω_c affected by a defect of domain Ω_d .

Fig. 1 Pancake and encircling probes with defect on the external surface

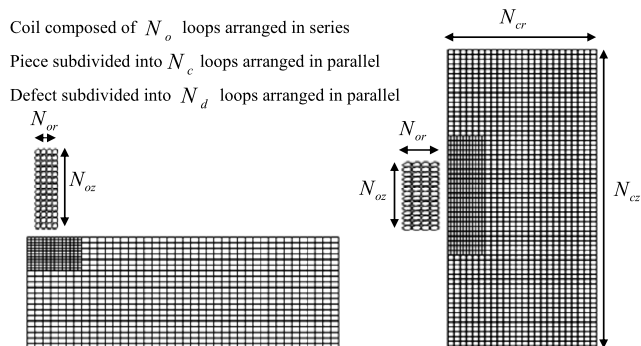
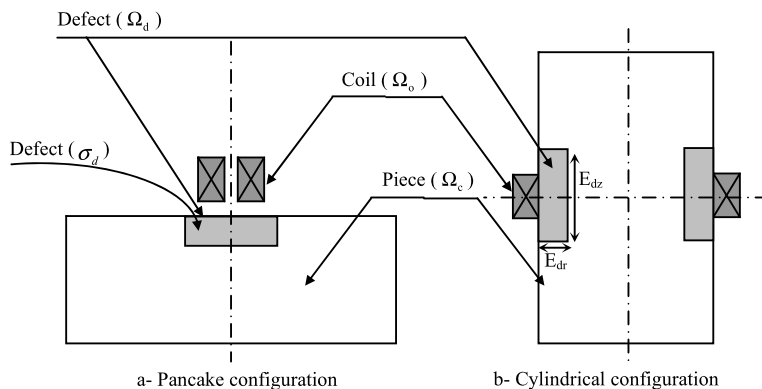


Fig. 2 Geometrical forms and meshing of the simplified models

The system is axially symmetric and the domain of solution is reduced to half of the device. Since the depth of penetration in the inductor is relatively big compared to the radius of the turn’s section, we admit, for the standard frequencies of control 100, 240 and 500 kHz, that the current density distribution in the latter is uniform. Therefore, the number of elements on the sensor is equal among turns of both reels. In other words, the number of elements is N_o distributed on N_{or} on the radial direction and N_{oz} on the axial one. The piece and the defect are, respectively, subdivided into $N_c(N_{cr}N_{cz})$ and $N_d(N_{dr}N_{dz})$ elementary loops as depicted in Fig. 2.

3.2 Equation in the Sensor

The presence of the induced currents in the piece and the defect influences the source current density J_{p_o} . To express this induction phenomenon, we apply Eq. (5) to turns p_o of electric conductivity σ_o .

$$\begin{aligned} \frac{2\pi r_{p_o}}{\sigma_{p_o}} J_{p_o} + j\omega\mu_o r_{p_o} \iint_{\Omega_o} G_{p_o q_o} J_{q_o} d\Omega_o \\ + j\omega\mu_o r_{p_o} \iint_{\Omega_c} G_{p_o q_c} J_{q_c} d\Omega_c \\ + j\omega\mu_o r_{p_o} (p_o) \iint_{\Omega_d} G_{p_o q_d} J_{q_d} d\Omega_d = u_{p_o} \end{aligned} \tag{8}$$

J_{p_o} and J_{q_o} are the current densities of the turns p_o and q_o belonging to the coil (Ω_o). J_{q_c} and J_{q_d} are the current densities of the turns q_c and q_d belonging to the charge (Ω_c) and the defect (Ω_d).

By considering that the sensor is subjected to a total voltage U , Eq. (8) becomes:

$$\begin{aligned} \sum_{p_o=1}^{N_o} \frac{2\pi r_{p_o}}{\sigma_{p_o} s_{p_o}} I_{p_o} + j\omega\mu_o I_o \sum_{p_o=1}^{N_o} r_{p_o} \sum_{q_o=1}^{N_o} G_{p_o q_o} \\ + j\omega\mu_o \sum_{p_o=1}^{N_o} r_{p_o} \sum_{q_c=1}^{N_c} G_{p_o q_c} s_{q_c} \sigma_{q_c} E_{q_c} \\ + j\omega\mu_o \sum_{p_o=1}^{N_o} r_{p_o} \sum_{q_d=1}^{N_d} G_{p_o q_d} s_{q_d} \sigma_{q_d} E_{q_d} = U \end{aligned} \tag{9}$$

s_{p_o}, s_{q_c} and s_{q_d} are respectively the turns sections of the coil, the charge and the defect. $\sigma_{p_o}, \sigma_{q_c}$ and σ_{q_d} are respectively the turns sections of the coil, the charge and the defect. r_{p_o} is the radius of the coil turns.

3.3 Equation in an Inspected Piece

To determine the induced electric field E_{p_c} in the inspected piece, we can apply Eq. (7) and write the following expression:

$$\begin{aligned} 2\pi E_{p_c} + j\omega\mu_o \sum_{\substack{q_c=1 \\ q_c \neq p_c}}^{N_c} G_{p_c q_c} s_{q_c} \sigma_{q_c} E_{q_c} \\ + j\omega\mu_o \sum_{q_d=1}^{N_d} G_{p_c q_d} s_{q_d} \sigma_{q_d} E_{q_d} \\ + j\omega\mu_o I_o \sum_{q_o=1}^{N_o} G_{p_c q_o} = 0 \end{aligned} \tag{10}$$

3.4 Equation in the Defect Region

The factors that exert an influence on electric conductivity are the temperature, the alloy composition and the residual stress. For this reason, we consider the defect as a local modification of electric conductivity (impurities, small burn, micro-solder. . .). This approach completes the coupled circuit models developed by several authors. Such models consider the defect as the loss of material [3–10].

Similarly, as in the tested piece, Eq. (7) is applied on the defect region. Hence, it yields the equation describing the induced electric field E_{pd} in the affected zone, as follows.

$$\begin{aligned} 2\pi E_{pd} + j\omega\mu_o \sum_{\substack{q_d=1 \\ q_d \neq p_d}}^{N_d} G_{p_d q_d} S_{q_d} \sigma_{q_d} E_{q_d} \\ + j\omega\mu_o \sum_{q_c=1}^{N_c} G_{p_d q_c} S_{q_c} \sigma_{q_c} E_{q_c} \\ + j\omega\mu_o I_o \sum_{q_o=1}^{N_o} G_{p_d q_o} = 0 \end{aligned} \tag{11}$$

3.5 Impedance Variation

The impedance is the ratio between the voltage U and the exciting current intensity I_o . The calculation approach of the impedance variation is very important for defect characterization [17]. It's the difference between the impedance $Z_d(\sigma_d \neq \sigma_c, N_d \neq 0)$ in presence of the flawed piece and that of the perfect one $Z_s(\sigma_d = \sigma_c, N_d = 0)$.

$$\Delta Z = Z_d - Z_s \tag{12}$$

We designate by (d) the state variable and the quantities related to the flawed piece.

From Eq. (9) and relation (12), we can finally deduce the expression of the impedance variation:

$$\begin{aligned} \Delta Z = j \frac{\omega\mu_o}{I_o} \sum_{p_o=1}^{N_o} r_{p_o} \left(\sum_{q_c^{(d)}=1}^{N_c-N_d} G_{p_o q_c^{(d)}} E_{q_c^{(d)}} \right. \\ \left. - \sum_{q_c=1}^{N_c} G_{p_o q_c} E_{q_c} \right) S_c \sigma_c \\ + j \frac{\mu_o \omega}{I_o} \sum_{p_o=1}^{N_o} r_{p_o} \sum_{q_d=1}^{N_d} G_{p_o q_d} S_d \sigma_d E_{q_d} \end{aligned} \tag{13}$$

This impedance variation can also be expressed according to defect electric conductivity (σ_d), radial and axial

depths (E_{dr} and E_{dz}) as defined below.

$$\begin{aligned} \Delta Z = j \frac{\omega\mu_o}{I_o} \sum_{p_o=1}^{N_o} r_{p_o} \left(\sum_{q_c^{(d)}=1}^{N_c-N_d} G_{p_o q_c^{(d)}} E_{q_c^{(d)}} \right. \\ \left. - \sum_{q_c=1}^{N_c} G_{p_o q_c} E_{q_c} \right) S_c \sigma_c \\ + j \frac{\mu_o \omega}{I_o N_d} \sum_{p_o=1}^{N_o} r_{p_o} \sum_{q_d=1}^{N_d} G_{p_o q_d} E_{dr} E_{dz} \sigma_d E_{q_d} \end{aligned} \tag{14}$$

The first term of Eq. (14) expresses the impedance variation that occurs by the loss of material (vacuum) and the modification of induced electric field distribution. The second one expresses the impedance variation that occurs by the induced electric field in the defect volume. We recall that the previous developed model does not express explicitly the defect characteristics as given in expression (14), but introduces the defect implicitly by removing the elementary turns of the affected region. Contrary, the proposed CEFM gives directly the impedance variation according to defect characteristics.

4 Validation of the Proposed CEFM

In order to check and validate this formulation, the obtained results using CEFM are compared with those of finite element method (FEM). For three excitation frequencies 100, 240 and 500 kHz, usually used in EC-NDT, we calculate the sensor impedance variation due to the presence of an axisymmetric defect in electric conductive plate. The sensor of 330 turns is an exciting coil of internal radius of 1 mm, of radial thickness of 0.75 mm and an axial length of 2 mm. The plate has a thickness of 1.55 mm and conductivity of 1 MS/m and is subdivided into 1000 elementary turns. 50 turns are according to the radial axis and 20 are according to the vertical axis. The defect has a thickness of 0.7525 mm, a radius of 1.5 mm and an electric conductivity of 1 MS/m (Fig. 3). Also, the defect is subdivided into 10 elementary turns according to the radial axis and 10 according to the vertical axis.

Our first objective is to validate the developed model while considering the defect with a finite electric conductivity. So, we calculate the impedance variation (ΔZ) using classic FEM and CEFM for a defect with electric conductivity of 0.000001 MS/m.

From Table 1, one can notice that the relative difference between the impedance variations calculated by the proposed model and those of FEM is very small and do not exceed 0.47 %; which means that the concordance between

Fig. 3 Piece with cylindrical defect on the superior face

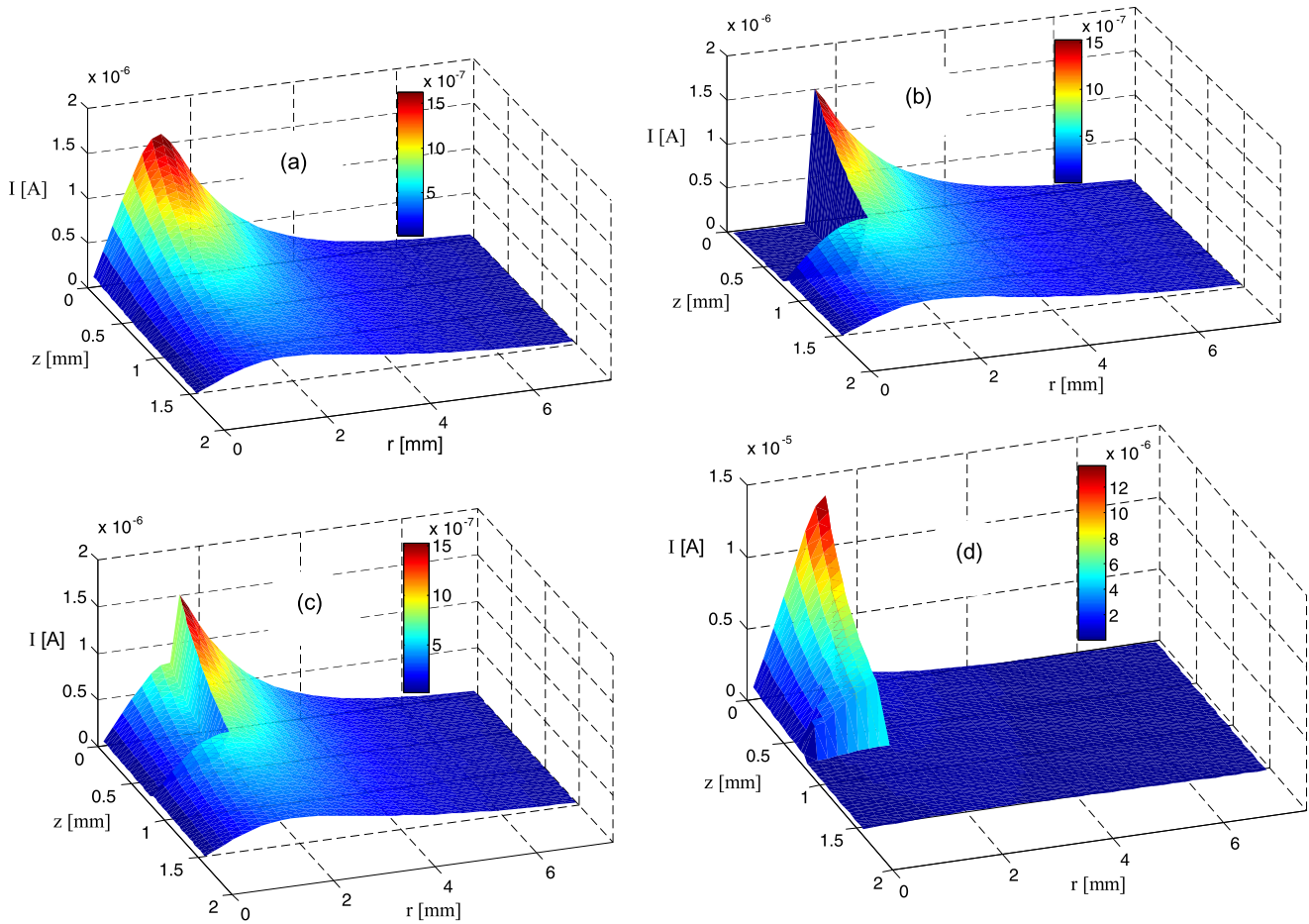
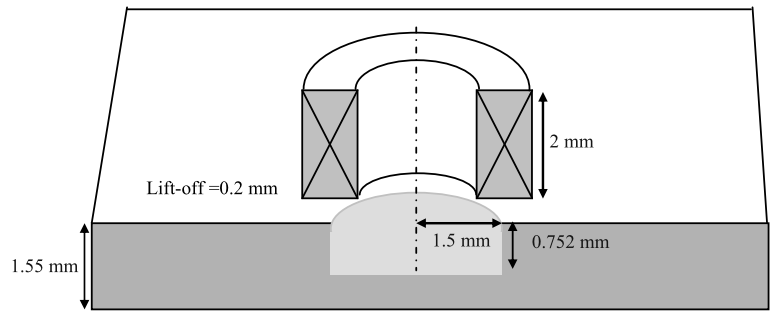


Fig. 4 Effect of defect electric conductivity on induced eddy currents, $f = 100$ kHz, (a): $\sigma_d = \sigma_c$, (b): $\sigma_d = 0$ MS/m, (c): $\sigma_d = 0.5\sigma_c$, (d): $\sigma_d = 10\sigma_c$

the results is very good and the model is hence validated. After validating the developed formula, we exploit the model to study the influence of defect characteristics.

5 Influence of Defect Characteristics

The purpose of the following simulations is to study the influence of defect, with rectangular cross section and parameters such as electric conductivity, radial depth and axial depth on the sensor impedance.

5.1 Defect Electric Conductivity

EC-NDT can detect impurities, small burn and micro-solder affecting locally electric conductivity [18–20]. The target of the next simulation is to study the influence of this defect physical parameter on induced eddy current trajectory and the sensor impedance. The studied device is the one treated previously (Fig. 3), but the defects differ by their electric conductivity while the other characteristics are fixed (cross section $S_d = 1.5 \times 0.752$ mm²). The external defect detec-

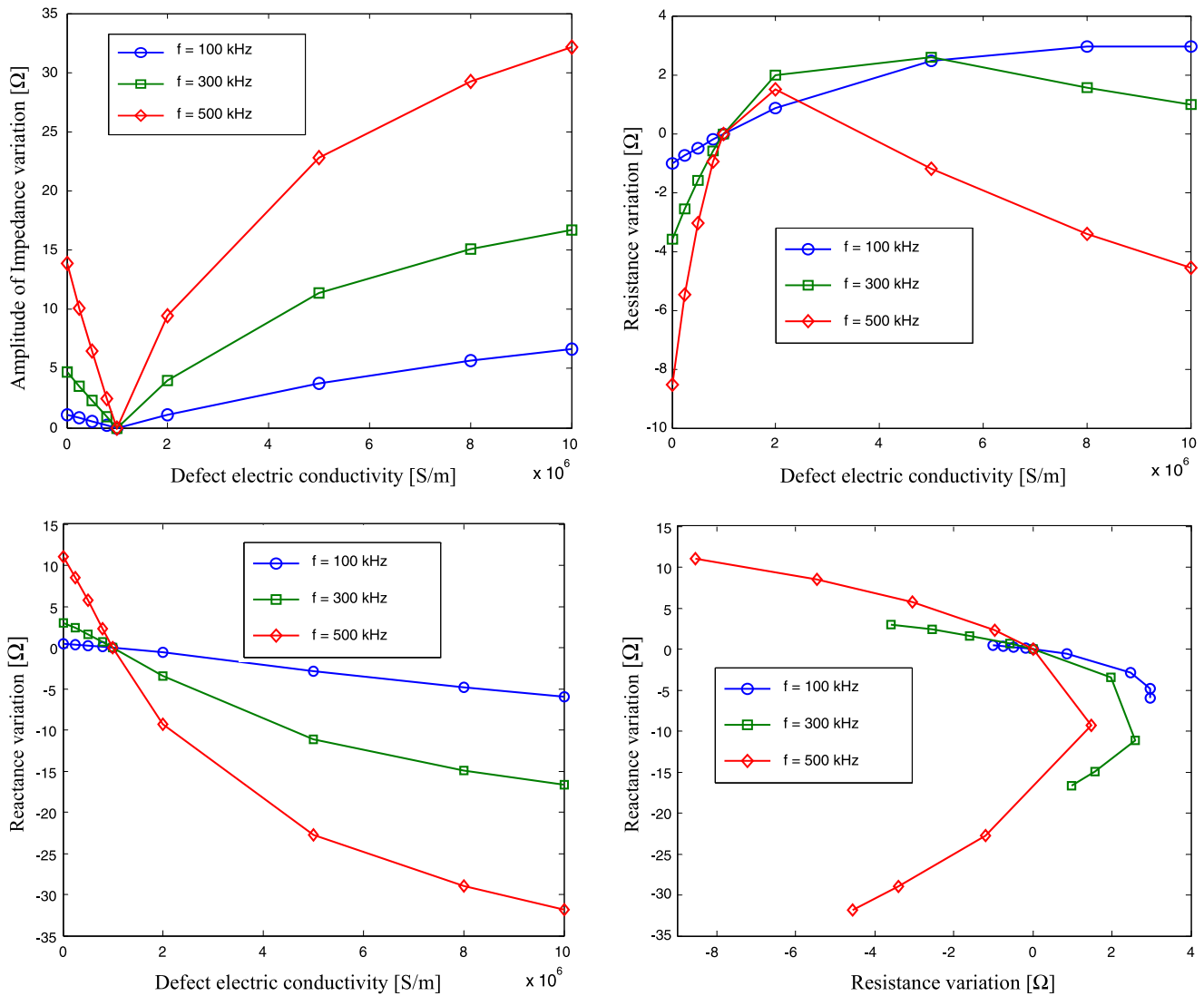


Fig. 5 Parameters of impedance variation according to defect electric conductivity

tion is treated by the calculation of the impedance variation at the ports of the sensor using the developed CEFM implanted in MATLAB environment. The results are summarised on Table 2.

In order to observe more clearly the effect of defect electric conductivity on induced eddy current distribution, we consider four kinds of defects (a, b, c and d) (Fig. 4).

From Table 2 and Fig. 4, we observe a great disruption of induced currents in the piece when the difference between electric conductivity of the affected and non affected region is significant (b and d); and weak in the case (c). This distortion is caused by the interaction between the alternating excitation current and the secondary electromagnetic quantities. The later are distorted by the presence of defects in the specimen and cause an apparent change in the impedance [1]. To demonstrate these effects on the measured quantities such as impedance variation, we calculate

the corresponding impedance for each defect electric conductivity while other defect parameters are fixed ($E_{dr} = 0.5$ mm, $E_{dz} = 2$ mm) (Fig. 5).

From Fig. 5, we can see that the impedance variation amplitude passes by three stages:

- $\sigma_d < \sigma_c$ The impedance variation parameters decrease when electric conductivity of defect increases.
- $\sigma_d > \sigma_c$ The impedance variation parameters increase when electric conductivity of defect increases.
- $\sigma_d = \sigma_c$ The impedance variation parameters are null.

These results can be interpreted by the difference in electric conductivity between the piece and the defect regions. When the difference in conductivity is significant, the defect signature will be also. When the two regions present the same electric conductivity, no signal is detected. We recall

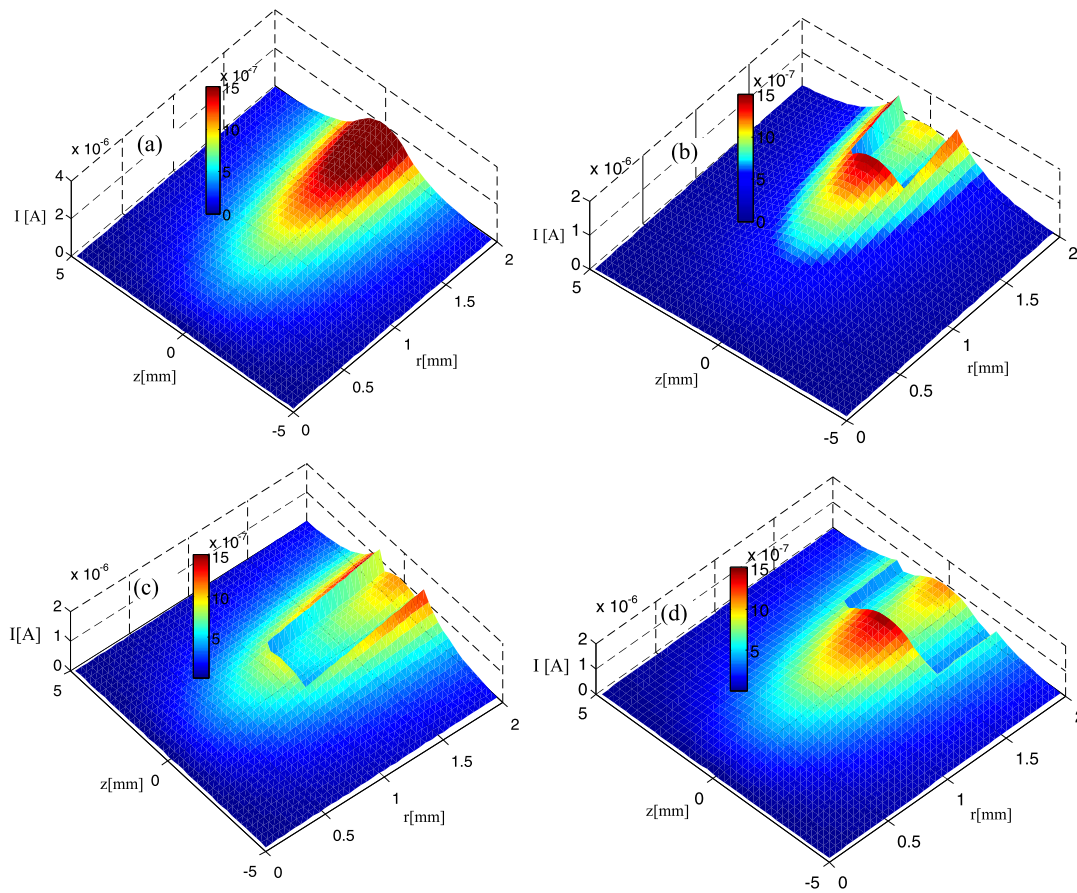


Fig. 6 Induced eddy current distribution. (A): $E_{dr} = 0$ mm, $E_{dz} = 0$ mm, (B): $E_{dr} = 0.5$ mm, $E_{dz} = 2$ mm, (C): $E_{dr} = 1$ mm, $E_{dz} = 2$ mm, (D): $E_{dr} = 0.5$ mm, $E_{dz} = 4$ mm

Table 1 Comparison of ΔZ calculated by finite element method (FEM) and CEFM in presence of the flawed plate ($\sigma_d = 1\text{MS/m}$)

Frequency (kHz)	100	240	500
ΔZ (FEM)	$-1.002 + 0.480i$	$-3.572 + 3.057i$	$-8.366 + 11.033i$
ΔZ (CEFM)	$-1.000 + 0.477i$	$-3.598 + 3.036i$	$-8.529 + 10.990i$
Relative error (%)	0.27	0.13	0.47

Table 2 Impedance variation ΔZ calculated for three kinds of defects for $f = 100$ kHz, and $\sigma_c = 1$ MS/m

Defect electric conductivity σ_d [MS/m]	$0\sigma_c$	$0.5\sigma_c$	$10\sigma_c$
Impedance variation ΔZ [Ω]	$-1.000 + 0.477i$	$-0.485 + 0.2591i$	$2.968 - 5.921i$

that other defect geometrical presenting a significant influence must be studied.

5.2 Study of the Influence of Defect Geometrical Parameters

This section will be devoted to the influence of defect shape and size affecting the impedance of an encircling coil at 100 kHz. The cylindrical EC-NDT system being studied is shown in Fig. 1b. The piece is a cylindrical rod of 2 mm ra-

dius, 10 mm length (-5 mm to 5 mm) and 1 MS/m electrical conductivity. The encircling coil of 59.6 MS/m is composed of $N_o = 330$ turns distributed over 30 turns following the axial direction and 11 turns following the radial one. It has an inner radius of 2.1 mm, an outer radius of 2.844 mm and a length of 2 mm. We can note that the mesh density depends strongly on the frequency. As well the frequency increases the mesh must be refined until the current density in the turn’s cross section becomes uniform. The affected region and the piece are regularly subdivided into 400 turns

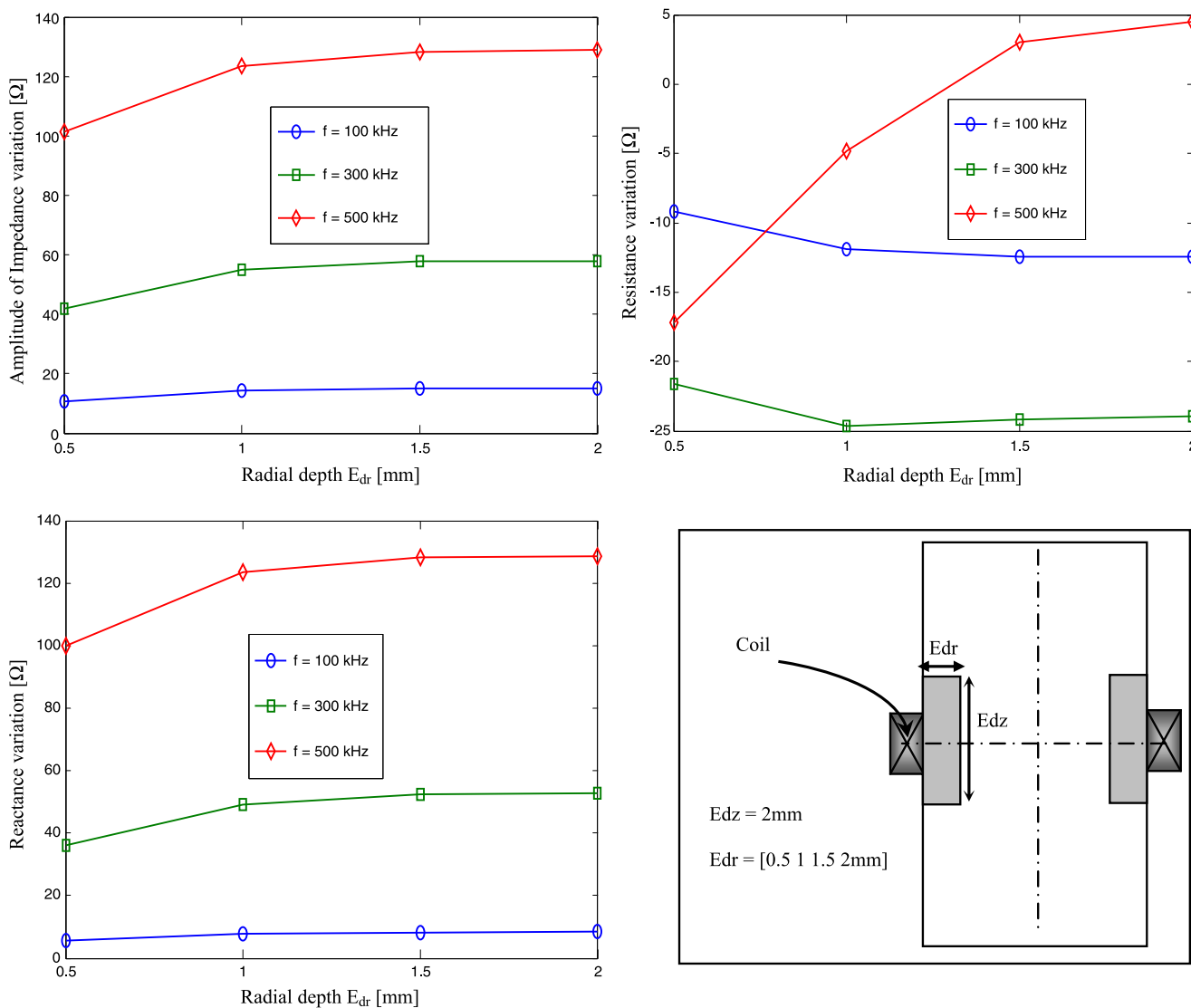


Fig. 7 Parameters of impedance variation according to defect radial depth. $E_z = 2$ mm, $\sigma_d = 0.5\sigma_c$

($N_c + N_d = 400$); although the values of N_c and N_d change for each defect size.

Equation (14) shows clearly that the impedance variation depends strongly on defect position and its geometrical parameters such as radial (E_{dr}) and axial (E_{dz}) depths. In addition, referring to Fig. 6, one can observe that the induced eddy current trajectory is perturbed by the presence of defect and this perturbation depends on the defect radial and axial depth as demonstrated by Eq. (14).

5.2.1 Impedance Variation According to Defect Radial Depth

By modifying the defect radial depth and setting its axial depth at 2 mm, we calculate the impedance parameters of the encircling coil. Figure 7 illustrates the impedance variations

due to an external defect presenting different radial depths (E_{dr}) for the frequencies of 100 kHz, 240 kHz and 500 kHz.

It is clear from Fig. 7 that the defect signature changes according to frequency and defect depth. In addition, the amplitude of the impedance variation increases when the defect depth increases, but changes slowly beyond $E_{dr} = 1$ mm, because beyond these depths the induced currents become feeble (Fig. 6c). For this reason, a higher perturbation is obtained for higher values of frequency and radial depth.

5.2.2 Impedance Variation According to Defect Axial Depth

Similar to the previous study, we set the radial depth at 0.5 mm and then we modify the axial depth from 1 mm to 10 mm. The yielded results are shown in Fig. 8.

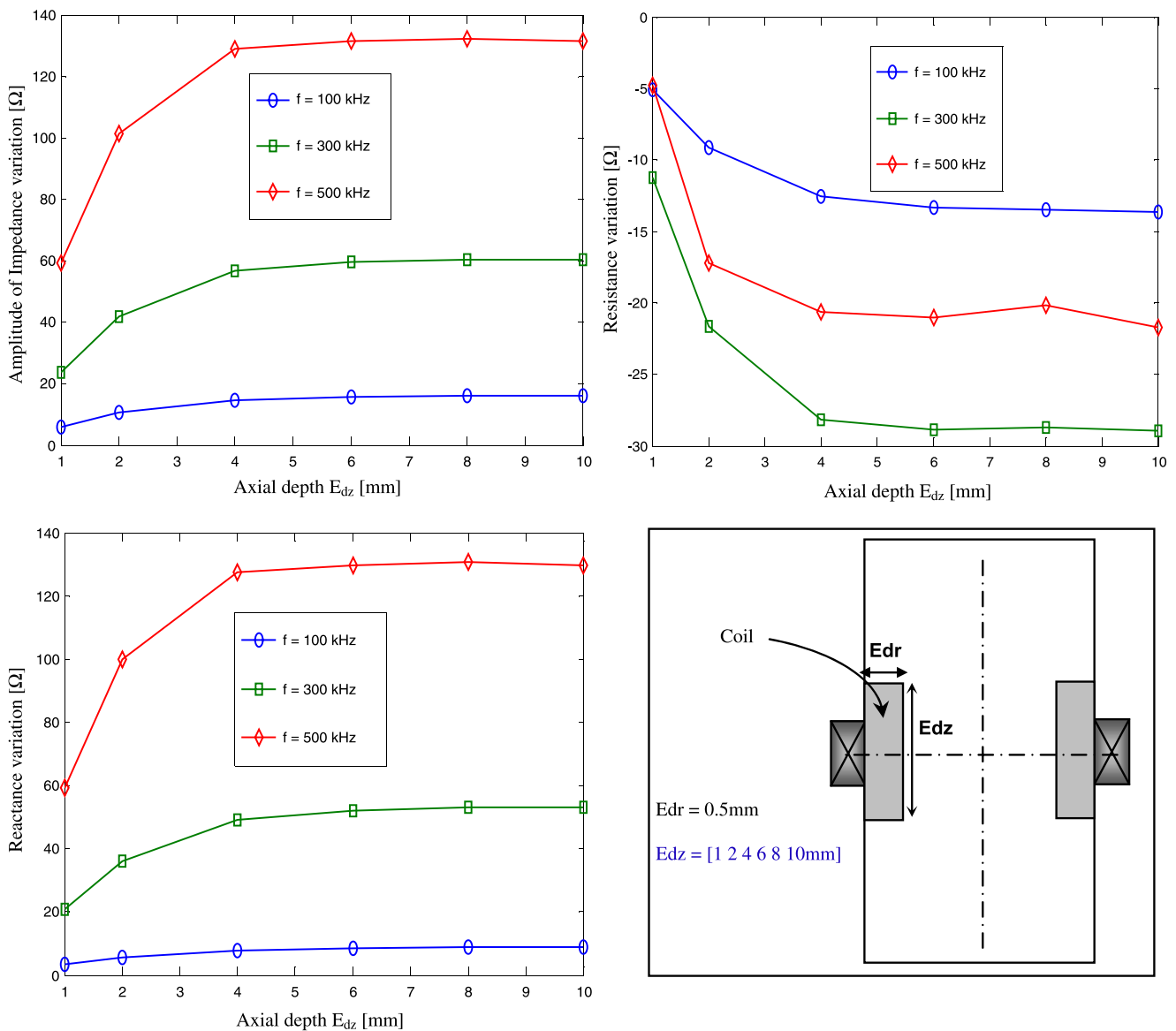


Fig. 8 Parameters of impedance variation according to defect axial depth. $E_{dr} = 0.5\text{ mm}$, and $\sigma_d = 0.5\sigma_c$

One can observe, in this case, that the impedance variation parameters increase when the defect axial depth increases but stabilize and become nearly constant beyond of $E_{dz} = 4\text{ mm}$ because of the axial skin effect (Fig. 6d). This effect limits the propagation of induced eddy current according to the axial direction and the coil sensor becomes less sensitive to the increase of the axial depth (beyond of $E_{dz} = 4\text{ mm}$). On another hand, the impedance variation amplitude becomes more important as the frequency gets higher.

5.3 Impedance Variation According to Defect Position

The Lissajous curves of the impedance are obtained for 10 positions of the sensor that corresponds to a 2 mm sensor

displacement step along a cylindrical rod of 20 mm axial length and electric conductivity of 1 MS/m. The defect is of radial depth of 0.5 mm, the axial depth of 2 mm and the electric conductivity of 0.5 MS/m. To get accurate results, the tested piece is regularly meshed into 1600 turns (very dense mesh). The resulted curves are depicted in Fig. 9. They illustrate the variations of the impedance parameters according to the displacement of the sensor along the cylindrical rod.

When the sensor is far from the defect, the impedance variations components (resistance, reactance, module and phase) are null. As the sensor approaches from the defect, we observe an increase in the variation of these components. We observe also, that a high frequency causes an increase of the induced currents being concentrated on the piece sur-

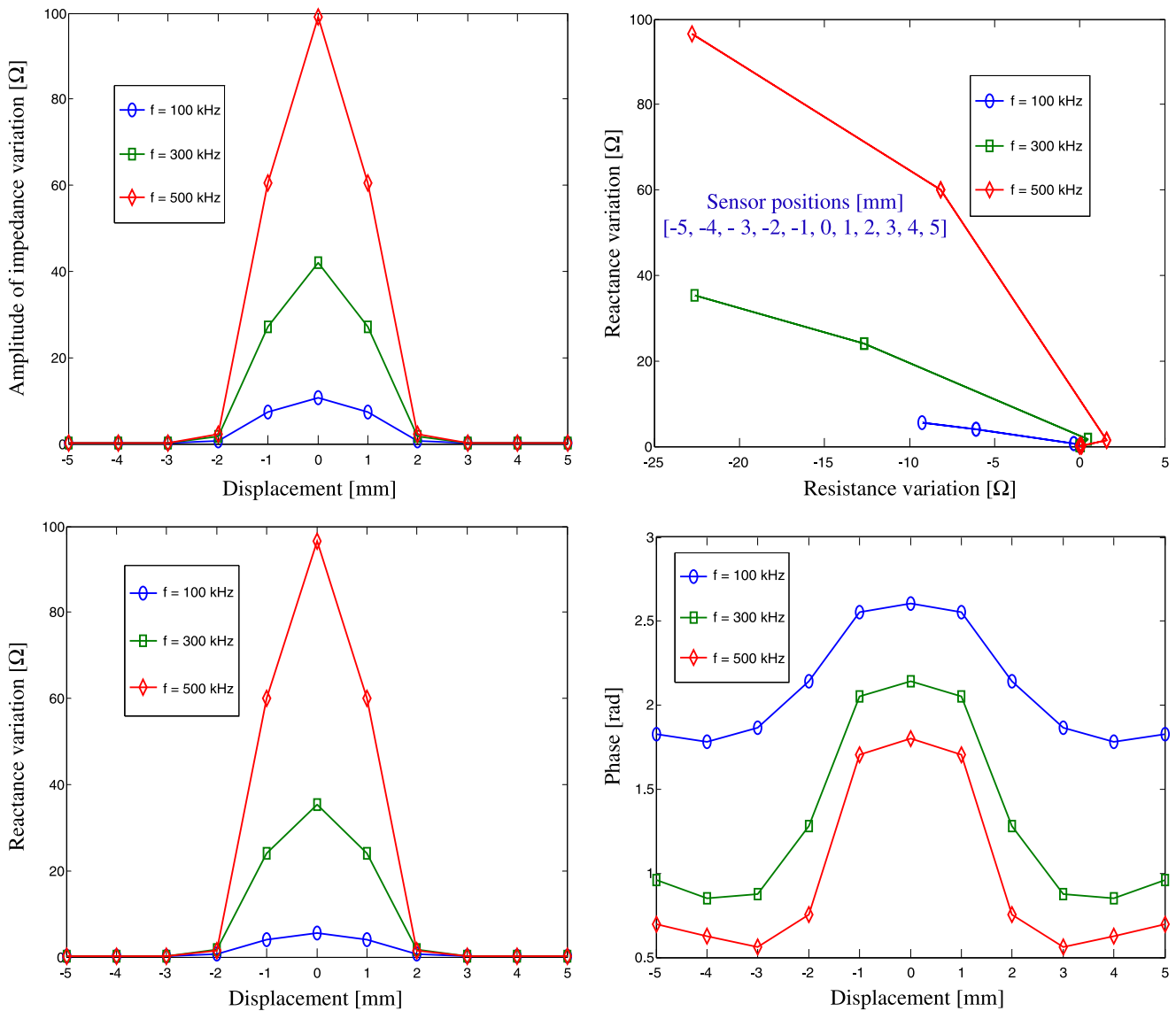


Fig. 9 Parameters of impedance variation according to defect position. $E_{dr} = 0.5$ mm, $E_{dz} = 2$ mm and $\sigma_d = 0.5\sigma_c$

face (skin effect) that becomes therefore more sensitive to the presence of an external defect.

6 Conclusion

Throughout this study, we have elaborated a direct semi analytical modeling of eddy current non destructive testing systems. The developed model, so called the coupled electric field approach, can be considered as an adaptation of the coupled electric circuit method [3–10] for the modeling of defect with finite electric conductivity. This approach has a great utility, since it permits expressing the semi-analytical impedance variation (defect signature) according to defect physical and geometrical characteristics (width, length, location and electric conductivity); and henceforth helping to

study clearly the influence of every parameter. More importantly, considering its short simulation time (depending on frequency and the size of the studied system), this method facilitates the resolution of inverse problem in real time, by expressing the defect characteristics according to the measured quantities [21, 22]. Besides, this quick and reliable simulation tool can provide a starting stage for the development of 3D phenomenological modeling of asymmetric EC-NDT configurations. Firstly, by the help of 3D finite element observation, we study the eddy current trajectory for every sensor position. The piece is discretized into elementary turns for which the shape and the size are given consistently according to the observation. Then, the geometrical functions (Green's function) are calculated and parameterized. While introducing the properties of every region, the

induced currents and the impedance variation are calculated in the same manner as in 2D.

References

- Javier, G.-M., Jaime, G.-G., Ernesto, V.-S.: Non-destructive techniques based on eddy current testing. *Sens. J.* 2525–2565 (2011)
- Lunin, V.P.: Phenomenological and algorithmic method for the solution of inverse problem of electromagnetic testing. *Russ. J. Non-destruct. Test.* **42**, 353–362 (2006)
- Maouche, B., Feliachi, M.: A half analytical formulation for the impedance variation in axisymmetrical modeling of eddy current non destructive testing. *Eur. Phys. J. Appl. Phys.* **33**, 59–67 (2006)
- Maouche, B., Feliachi, M.: Analyse de l'effet des Courants induits sur l'impédance d'un système électromagnétique alimenté en tension BF ou HF. Utilisation de la méthode des circuits couplés. *J. Phys. III* **10**, 1967–1973 (1997)
- Maouche, B., Rezak, A., Feliachi, M.: Semi analytical calculation of the impedance of differential sensor for eddy current non destructive testing. In: *NDT & E International*, vol. 42, pp. 573–580. Elsevier, Amsterdam (2009)
- Bouziidi, A., Maouche, B., Feliachi, M., Berthiau, G.: Pulsed eddy current non-destructive evaluation based on coupled electromagnetic quantities method. *Eur. Phys. J. Appl. Phys.* **57**, 10601 (2012) (9 pages)
- Amrane, S., Latreche, M.E.H., Feliachi, M.: Coupled circuits model combined with deterministic and stochastic algorithms for the inductor design. *Int. J. Appl. Electromagn. Mech.* **32**, 195–206 (2010)
- Mouhalebi, H., Bouali, F., Feliachi, M.: Use of half analytical method for detection of defects in diet pulses. In: *The 15th International Workshop on Electromagnetic Non Destructive Evaluation, ENDE 2010, Szczecin, Poland* (2010)
- Zerguini, S., Maouche, B., Latreche, M., Feliachi, M.: A coupled fictitious electric circuit's method for impedance of a sensor with ferromagnetic core calculation. Application to eddy currents non destructive testing. *Eur. Phys. J. Appl. Phys.* **48**, 31202 (2009) (6 pages)
- Doirat, V.: Contribution à la modélisation des systèmes de contrôles non destructifs par Courants de Foucault, application à la caractérisation physique et dimensionnelle de matériaux de l'aéronautique. Doctorate Thesis, Nantes, France (2007)
- Theodoulidis, T.P., Bowler, J.R.: Bobbin coil signal variation due to an axisymmetric circumferential groove in a tube. *AIP Conf. Proc.* **1096**, 1922–1929 (2008)
- Lemistre, M.B., Balageas, D.L.: Hybrid electromagnetic method for NDE of GFRP and CFRP composites materials. In: *Health Monitoring and Smart Nondestructive Evaluation of Structural and Biological Systems IV*, vol. 5768, San Diego (2005)
- Yamada, S.: High-spatial-resolution magnetic-field measurement by giant magnetoresistance sensor—applications to nondestructive evaluation and biomedical engineering. *Int. J. Smart Sens. Intell. Syst.* **1**(1) (2008)
- Shiraishi, K., Izumida, M., Murakami, K.: Estimation of depth and volume for defects by eddy current testing. *Electr. Eng. Jpn.* **127**(4), 29–38 (1999)
- Bernieri, A., Ferrigno, L., Molinara, M.: Crack shape reconstruction in eddy current testing using machine learning systems for regression. *IEEE Trans. Instrum. Meas.* **57**(9) (2008)
- Van Bladel, J.: *Electromagnetic Field*. Wiley-IEEE Press, New York (2007)
- Yating, Y., Pingan, D., Luchuan, X.: Coil impedance calculation of an eddy current sensor by the finite element method. *Russ. J. Nondestruct. Test.* **44**(4), 296–302 (2008)
- Cacciola, G., Calcagno, S., Megali, G., Pellican, D., Versaci, M., Morabito, F.C.: Eddy current modelling in composite materials. *PIERS Online* **5**, 591–595 (2009)
- Hillmann, S., Heuer, H., Baron, H.-U., Bamberg, J., Yashan, A., Meyendorf, N.: Near surface residual stress-profiling with high frequency eddy current conductivity measurement. In: *Proceedings of the 35th Annual Review of Progress in Quantitative Non-destructive Evaluation*, vol. 1096, pp. 1349–1355 (2008)
- Yu, F., Peter, B.: Simple analytical approximations for eddy current profiling of the near-surface residual stress in shot-peened metals. *J. Appl. Phys.* **96**, 1257–1266 (2004)
- Shao, K.R., Youguang, G., Lavers, J.D.: Multiresolution analysis for reconstruction of conductivity profiles in eddy current non-destructive evaluation using probe impedance data. *IEEE Trans. Magn.* **40**, 2101–2103 (2004)
- Yokose, Y., Cingoski, V., Yamashita, H.: Genetic algorithms with assistant chromosomes for inverse shape optimization of electromagnetic devices. *IEEE Trans. Magn.* **36**, 1052–1056 (2000)